

# Simultaneously Solving Swarms of Small Sparse Systems on SIMD Silicon

Bryce Adelstein Leibel, Hans Johansen, and Samuel Williams  
Lawrence Berkeley National Laboratory, Computational Research Division  
bryceleibel@gmail.com, {hjohansen, swwilliams}@lbl.gov

**Abstract**—A number of computational science algorithms lead to discretizations that require a large number of independent small matrix solves. Examples include small non-linear coupled chemistry and flow systems, one-dimensional sub-systems in climate and diffusion simulations and semi-implicit time integrators, among others. We introduce an approach for solving large quantities of independent banded matrix problems on SIMD architectures. Unlike many vectorized or batched approaches that rely on reusing the matrix factorization across multiple solves, our algorithm supports batches of matrices that differ (due to spatial variation or non-linear solvers, for example). We present an implementation of our approach for diagonally-dominant tridiagonal systems that is optimized via compiler directives, tiling, and choice of data layout. Performance is evaluated on three Intel micro-architectures with different cache, vectorization, and threading features: Intel Ivy Bridge, Haswell, and Knight’s Landing. Finally, we show that our solver improves on existing approaches and achieves ~90% of STREAM Triad effective bandwidth on all three platforms.

**Keywords**—Vector, SIMD, AVX512, Many-core, Xeon Phi, Knight’s Landing, KNL, Batched, Banded, Linear Algebra, Sparse, Matrix, Tridiagonal, Tridiagonal Matrix Algorithm, TDMA, Thomas Algorithm, Layout, Tiling

## I. INTRODUCTION

One important class of problems in computational science is solving smaller-dimensional matrix sub-systems that are duplicated across many degrees of freedom in a larger two (or more) dimension computation. Such problems appear in pointwise chemistry systems in the context of larger flow simulations (found in cloud microphysics [1] and combustion [2] models), one-dimensional systems that represent a numerically stiff direction for a physical phenomenon (found in atmospheric radiation [3], groundwater penetration [4] and cloud convection [5] models) and implicit solvers that need to couple these kinds of sub-systems (such as semi-implicit time integrators [6]). In most cases, these matrices are small -  $O(30 - 100)$  vertical levels in a climate application, for example.

Because these sub-systems are often non-linear matrix systems with space- and time-dependent entries, these applications may not use a “factor once, solve many times” approach that seeks to amortize setup and factorization costs across multiple right-hand sides. This strategy is used by many linear algebra libraries. For example, the LAPACK routines `dptsv`, `dtsvb`, `dgtsv` and `dgttrs` [7] use this approach. In our case, it is usually sub-optimal on Single Instruction Multiple Data (SIMD) CPU, SIMD many-core and Single Instruction Multiple Thread (SIMT) GPGPU architectures to simply call an optimized general-purpose linear algebra library, such as Intel’s Math Kernel Library (MKL) [7] or NVIDIA’s CUDA BLAS library (cuBLAS) [8]. These libraries may

not achieve peak performance for batch solves of small matrices because they are not designed to simultaneously solve multiple systems and take advantage of the data locality and vectorization opportunities exposed by such interleaving.

We have developed a model problem that mimics the conditions encountered in these kinds of large-scale simulations. Key aspects of the test problem include:

- A 3D Cartesian grid  $((i, j, k)$  indices), where different matrix systems in the **vertical dimension**  $k$  are generated at each **horizontal coordinate**  $(i, j)$  and the extent of  $k$  is  $O(30 - 100)$ .
- Each matrix is **diagonally-dominant**, **tridiagonal**, and must be solved for all values in the  $k$  dimension.
- The matrix is derived from a finite difference discretization for the 1D diffusion equation that can be solved **without pivoting**.

In §III, we describe the **Simultaneous Streaming Thomas Algorithm (SSTA)**, which is designed to solve this class of problems. The algorithm computes the solution to multiple systems simultaneously, promoting data locality and facilitating the use of vector instructions. Additionally, SSTA iterates through memory in unit stride to enable hardware prefetching facilities to easily track the streams of memory accessed. SSTA supports different data layouts and tiling schemes, and we demonstrate how they can significantly influence performance. In §V, we compare performance against a baseline solver derived from a production climate code that utilizes Intel MKL and STREAM Triad [9]. Results show that SSTA achieves a ~2x speedup over the MKL solver on Ivy Bridge and Haswell, a ~12x speedup on Knight’s Landing, and attains ~90% of STREAM Triad effective bandwidth on all three platforms.

## II. RELATED WORK

Approaches to solving large numbers of small matrices have been developed before in a variety of contexts. Libraries like Blaze [10], [11], LIBXSMM [12], [13], Intel’s MKL [7] and NVIDIA’s cuBLAS [8] support batched computation of sparse and dense matrices. Many implementations only support batched solves where the same matrix is applied to multiple right hand sides. As we demonstrate, this approach fails to expose vector parallelism in our case. Pipelined and batched versions of the Thomas algorithm [14], LU factorization [15] and similar algorithms that interleave the solution of multiple matrices exist, but most target SIMT GPGPU platforms, not SIMD architectures.

There are few solutions that are designed to support different data layouts and tiling schemes, target both SIMD

and SIMT architectures, and simultaneously solve many small problems that do not share the same matrix.

### III. IMPLEMENTATION

Suppose we have a  $nk \times nk$  **diagonally-dominant tridiagonal matrix**  $A$  and two  $nk$  element vectors  $u^s$  and  $u^{s+1}$ . We wish to solve  $Au^{s+1} = u^s$  for  $u^{s+1}$ :

$$\begin{bmatrix} b_0 & c_0 & & & 0 \\ a_1 & b_1 & c_1 & & \\ & a_2 & b_2 & \dots & \\ & & \dots & \dots & c_{nk-2} \\ 0 & & & a_{nk-1} & b_{nk-1} \end{bmatrix} \begin{bmatrix} u_0^{s+1} \\ u_1^{s+1} \\ \dots \\ \dots \\ u_{n-1}^{s+1} \end{bmatrix} = \begin{bmatrix} u_0^s \\ u_1^s \\ \dots \\ \dots \\ u_{n-1}^s \end{bmatrix} \quad (1)$$

Our matrix  $A$  is stored as three vectors: an  $nk - 1$  element sub-diagonal vector  $a$ , an  $nk$  element diagonal vector  $b$  and an  $nk - 1$  element super-diagonal vector  $c$ .

#### A. The Thomas Algorithm

We can use a simplified form of Gaussian elimination that does not require pivoting, known as the **Thomas algorithm** or the **tridiagonal matrix algorithm (TDMA)** [16], to solve the type of system described by Equation 1. The Thomas algorithm takes advantage of sparsity to be  $O(nk)$  in time, and can be extended to banded matrices and LU factorizations. It is also a significant improvement over dense Gaussian elimination, which is  $O(nk^3)$  in time. We use a formulation of the Thomas algorithm that does not require any storage for temporary values, but overwrites the  $b$  vector and solves for  $u^{s+1}$  in place (overwriting  $u^s$ ).

The Thomas algorithm consists of two passes. First, a **forward pass** is performed to **eliminate** the  $a_k$  elements:

---

```
for (auto k = 1; k < nk; ++k) {
    auto const m = a[k] / b[k - 1];
    b[k] -= m * c[k - 1];
    u[k] -= m * u[k - 1];
}
```

---

Then, an abbreviated form of **back substitution** is performed to obtain the solution:

---

```
u[nk - 1] = u[nk - 1] / b[nk - 1];

for (auto k = nk - 2; k >= 0; --k)
    u[k] = (u[k] - c[k] * u[k + 1]) / b[k];
```

---

The Thomas algorithm has very low **arithmetic intensity (AI)** [17]. During the course of our work, we developed a **theoretical peak performance model** for the Thomas algorithm.

First, we count the number of floating point operations (FLOPs) performed. We will consider multiplication, addition and division operations as FLOPs. Each iteration of the forward elimination loop contains 1 division, 2 multiplications and 2 subtractions. This gives us a total of either  $3(nk - 1)$  FLOPs on fused-multiply-add (FMA) architectures [18] or  $5(nk - 1)$  FLOPs on non-FMA architectures. Next, the pre-substitution operation (the assignment to  $u[nk - 1]$  in the back substitution loop) performs a single division. Finally, the back substitution loop performs 1 multiplication, 1 subtraction and 1 division, adding either  $2(nk - 1)$  FLOPs (FMA architectures) or  $3(nk - 1)$  FLOPs

(non-FMA architectures). In total, this gives us either  $5nk - 4$  FLOPs (FMA) or  $8nk - 7$  FLOPs (non-FMA) for the entire Thomas algorithm.

Next, we must determine the amount of data movement that occurs in the Thomas algorithm. We start by assuming that we will achieve optimal performance when  $a$ ,  $b$ ,  $c$  and  $u$  are cached in between the forward elimination loop and the back substitution loop.

The Thomas algorithm accesses four arrays, reading from all of them and writing to two of them ( $b$  and  $u$ ).  $b$  and  $u$  have extent  $nk$ , so we store  $2nk$  elements.  $a$  and  $c$  have extent  $nk - 1$ , so we load  $2(nk - 1) + 2nk$  elements. In total,  $6nk - 2$  elements are moved. Assuming 8 byte elements (e.g. double precision),  $48nk - 16$  bytes are moved to and from main memory during execution of the Thomas algorithm.

This gives us a FLOPs/byte ratio of  $(5nk - 4)/(48nk - 16)$  (FMA) or  $(8nk - 7)/(48nk - 16)$  (non-FMA). The lower bound for arithmetic intensity is  $1/32$  FLOPs/byte when  $nk = 1$ . The upper bound is  $5/48$  FLOPs/byte (FMA) or  $1/6$  FLOPs/byte (non-FMA) as  $nk$  approaches infinity. Based on this analysis, we can conclude that the Thomas algorithm is **memory-bandwidth bound**. Thus, we use effective bandwidth, not FLOPs, as our performance metric.

We verified our analytic model by measuring hardware performance counters that track memory traffic with the Intel VTune Amplifier XE profiler [19]. We found that memory bandwidth measured via hardware counters generally agreed with our model.

#### B. Batching and Vectorization

In the applications described in §I we need to apply the Thomas algorithm to each vertical column in a  $ni \times nj \times nk$  3D Cartesian grid, where  $i$  and  $j$  are **horizontal dimensions** and  $k$  is the **vertical dimension**. These computations are known as **vertical solves**. Since each vertical solve is independent of the others, this is an embarrassingly parallel problem. The matrix coefficients for each column depend on the problem state, so a unique matrix needs to be constructed before each solve. There are two different approaches to computing these batch solves.

The most straightforward approach is to solve each column independently (the **independent solve strategy**; Figure 1). An  $nk \times nk$  tridiagonal matrix is constructed for each vertical column, and then the Thomas algorithm is used to solve the linear system formed by the matrix and the column. Because the vertical solves are independent, they can be executed concurrently via task-level parallelism. Vectorization of the  $nk$  loop is not possible as each iteration of the loops in the Thomas algorithm depends on the prior iteration (e.g. loop-carried dependencies) [14]. Even if it was possible to vectorize in the vertical dimension  $k$ , it would still be undesirable to do so. The extent of the vertical dimension is small enough in the applications we are concerned with -  $O(30 - 100)$  - that it inhibits vectorization as well.

The other approach is to simultaneously solve multiple columns (the **simultaneous solve strategy**; Figure 2). A block  $nk \times nk$  tridiagonal matrix is constructed for the whole grid; each block contained within the matrix is an  $ni \times nj$  horizontal plane. To perform the vertical solves, we view the

**Figure 1: Independent Solve Strategy:** A vertical column of  $nk$  elements is extracted from a  $ni \times nj \times nk$  3D Cartesian grid and used as the right-hand side in a tridiagonal linear system. The system for each column is solved independently from other columns. This approach exposes task parallelism, but vectorization is not possible in the vertical dimension  $k$  due to its small extent and the loop-carried dependencies present in the Thomas algorithm [14]. This strategy is used by our MKL baseline solver.

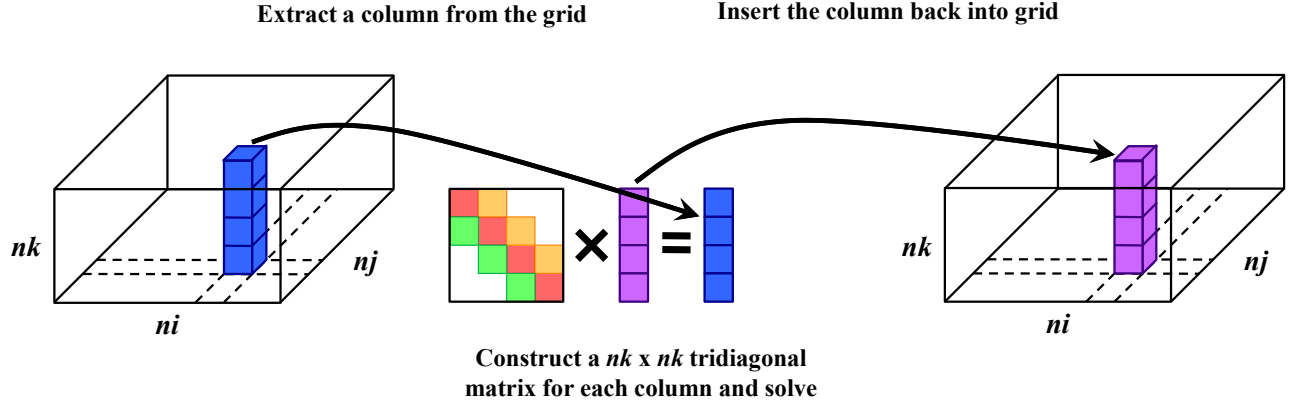
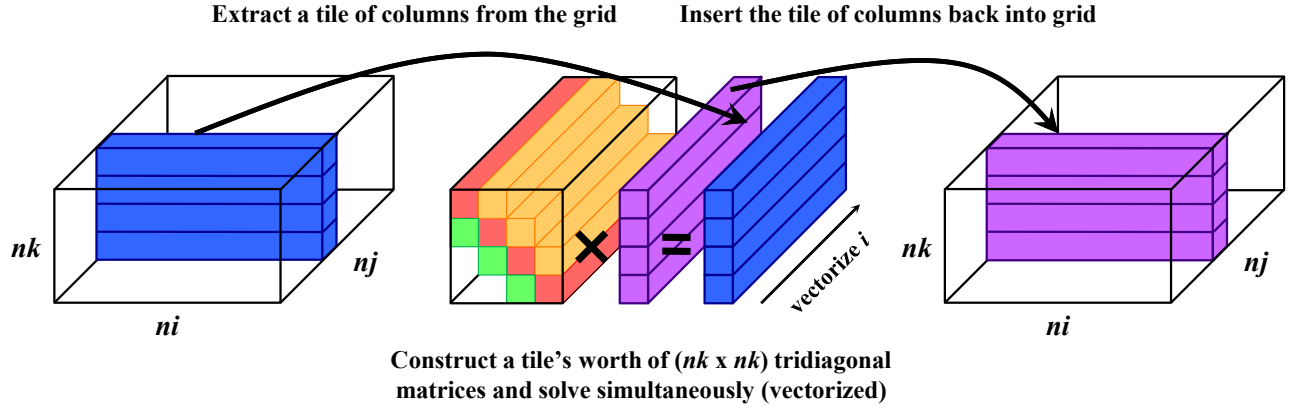


**Figure 2: Simultaneous Solve Strategy:** A tile of vertical columns, each containing  $nk$  elements, is extracted from a  $ni \times nj \times nk$  3D Cartesian grid. All the columns in the tile are solved simultaneously, interleaving the computation of individual solves. This approach exposes task parallelism, exhibits good data locality and enables vectorization in one of the horizontal dimensions ( $i$  in this case). SSTA uses this strategy.



entire 3D grid as an  $nk$  block vector of  $ni \times nj$  planes and apply it to the block matrix. Each step of the algorithm is applied across an entire plane. The forward pass becomes:

```
for (auto k = 1; k < nk; ++k)
  for (auto j = 0; j < nj; ++j)
    for (auto i = 0; i < ni; ++i) {
      auto const m = a[i][j][k] / b[i][j][k - 1];
      b[i][j][k] -= m * c[i][j][k - 1];
      u[i][j][k] -= m * u[i][j][k - 1];
    }
```

This approach facilitates both task-level parallelism and vectorization. The grid can be tiled into smaller sub-grids, and the Thomas algorithm can be applied to each sub-grid independently. Each step of the Thomas algorithm can be vectorized across the  $ni \times nj$  horizontal plane that it is operating on: e.g. the  $i$  or  $j$  loop in the above snippet can be vectorized.

The vector parallelism exposed by the simultaneous approach offers a major benefit over the independent approach. It is necessary to vectorize even for a memory-bandwidth bound problem like the Thomas algorithm, as peak memory

bandwidth cannot be achieved without exploiting wider vector loads and stores.

Our MKL baseline solver uses the independent solve approach, while SSTA uses the simultaneous solve strategy.

### C. Data Layout

The data layout of the 3D Cartesian grid has a huge impact on the performance of our solver. Throughout the course of our research, our understanding of the impact of different data layouts has evolved substantially. We have investigated three different schemes:  $ijk$ ,  $kji$  and  $ikj$  (Table I).

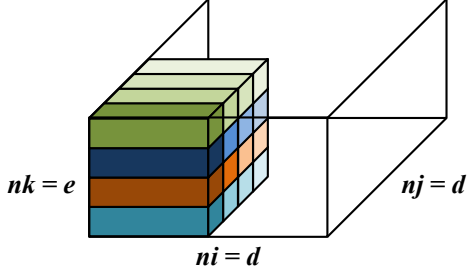
Table I: Data Layouts for the 3D Cartesian Grid

Name	$i$ -stride (Horizontal)	$j$ -stride (Horizontal)	$k$ -stride (Vertical)
$ijk$ , Column-Major	1	$ni$	$(ni)(nj)$
$kji$ , Row-Major	$(nj)(nk)$	$nk$	1
$ikj$	1	$(ni)(nz)$	$ni$

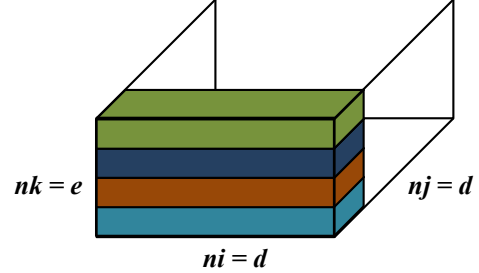
The production code that our MKL baseline solver is derived from uses the  $ijk$ -layout. The vertical columns that

**Figure 3: Example of Different Layouts and Tiling Schemes:** The SSTA solver supports four layout and tiling scheme combinations. The figures below show how the different combinations would partition an  $d \times d \times e$  grid into four tiles each containing  $(d^2/4)(e)$  elements (one tile is shown). With the tile- $ij$  scheme we get  $d/2 \times d/2 \times e$  tiles, and with the tile- $j$  scheme we get  $d \times d/4 \times e$  tiles. Different colors indicate different contiguous regions within the tile. Regions with similar colors have greater locality with each other.

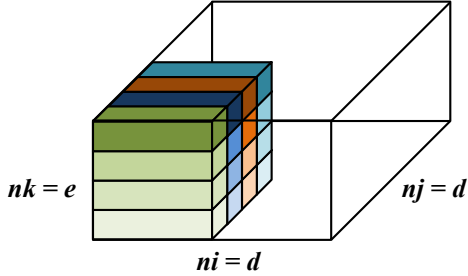
(a) *ijk*-Layout with the Tile- $ij$  Scheme:  $(d/2)(e)$  contiguous  $i$ -rows each containing  $d/2$  elements. This layout and tiling combination exhibits the least contiguity for the *ijk*-layout.



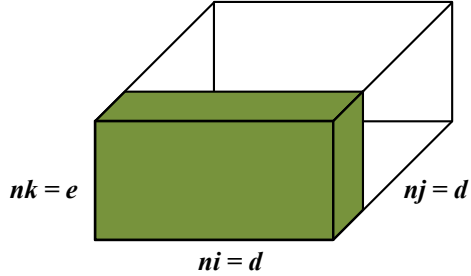
(b) *ijk*-Layout with the Tile- $j$  Scheme:  $e$  contiguous  $ij$ -planes, each containing  $d^2/4$  elements. This layout and tiling combination exhibits the greatest contiguity for the *ijk*-layout.



(c) *ikj*-Layout with the Tile- $ij$  Scheme:  $(d/2)(e)$  contiguous  $i$ -rows each containing  $d/2$  elements. This layout and tiling combination exhibits the least contiguity for the *ikj*-layout.



(d) *ikj*-Layout with the Tile- $j$  Scheme: One contiguous region containing  $(d^2/4)(e)$  elements. This layout and tiling combination exhibits the greatest contiguity out of the four options.



we need to pass in to MKL as right-hand sides are non-contiguous, as the vertical dimension  $k$  is the dimension with the greatest stride. Currently, the production codebase allocates a temporary buffer, copies data from the grid into the buffer, calls the LAPACK solver and then copies the result from the buffer back to the grid.

We have found the  $kji$ -layout to be optimal for our MKL baseline solver. With the  $kji$ -layout, we have contiguous vertical columns that can be passed to MKL without temporary allocations or unnecessary copies. We observed a noticeable performance increase from this optimization with very little source code change, although we have not studied the impact of this layout change on other components in more complex multi-kernel applications.

Our SSTA solver uses either the *ijk*- or *ikj*-layout. SSTA vectorizes in one of the horizontal dimensions ( $i$ ), so it is desirable to use layouts where the horizontal dimension that we are vectorizing is the unit stride dimension, avoiding strided vector loads. The *ikj*-layout arose as an optimization to combat data locality, translation-lookaside buffer (TLB) and prefetching issues on Knight's Landing, and is described in greater detail in the next section and in §V-A.

#### D. Tiling

To ensure good cache utilization, it is often necessary to break a larger grid into smaller **tiles** that better amortize

nested loop overheads, expose greater data locality and keep data resident in a particular level of the cache hierarchy [20]. This technique is also known as **cache blocking**. Additionally, partitioning a grid with dimensions known only at application initialization into fixed size tiles can provide some of the performance benefits of compile-time-fixed dimensions while retaining the flexibility of a dynamically-sized problem [21]. Tiling also provides a useful abstraction for parallel work distribution.

The production code that our MKL baseline solver is derived from is not task parallelized or explicitly tiled. Since each column is solved independently, there is little opportunity to improve data locality and reuse via tiling (described in §V-A). Conceptually, since each column is solved independently in the production code, it is **effectively** tiled, albeit with a very small tile size (a single column). Our MKL baseline solver is tiled solely to facilitate task parallelization.

On the other hand, tiling is very fundamental to our SSTA solver. Our performance model (§III-A) is based on caching assumptions that we rely on tiling to enforce. In particular, we assume that all four arrays ( $a$ ,  $b$ ,  $c$  and  $u$ ) remain in the cache hierarchy in between the loops of the kernel. If any of these four arrays need to be reloaded from main memory, the amount of data movement is significantly increased and the arithmetic intensity of the algorithm decreases dramatically.

On the platforms covered in this paper, we typically aim to fit within the L2 cache. While our untiled SSTA results outperform the MKL baseline results, they were well below the manufacturer-specified bandwidth and STREAM Triad effective bandwidth (Figure 6).

It is important to note the distinction between **per-array tile size** (e.g. the tile size for one of the four arrays) and the **total tile size** (e.g. the sum of the per-array tile sizes). The total tile size is the amount of data we need to remain in cache in between the forward elimination loop and the back substitution loop. Unless stated otherwise, when we refer to “tile size” we mean total tile size.

Due to the loop-carried dependencies in the Thomas algorithm and the small extent of  $nk$ , we could not tile the vertical dimension. So, we explored two tiling schemes that partition the horizontal  $ij$ -plane.

The **tile- $ij$  scheme** partitions both the  $i$  and  $j$  dimensions, yielding tiles with arbitrary horizontal shape consisting of contiguous  $i$ -rows. The **tile- $j$  scheme** partitions only the  $j$  dimension, producing tiles consisting of contiguous  $ij$ -planes. There is a trade-off between these two schemes, with the tile- $ij$  scheme offering greater flexibility in tile size and the tile- $j$  scheme offering greater contiguity.

For example, suppose we partition a  $d \times d \times e$   $ijk$ -layout grid into four tiles each containing  $(d^2/4)(e)$  elements, with the tile- $ij$  scheme producing  $d/2 \times d/2 \times e$  tiles (Figure 3a) and the tile- $j$  scheme producing  $d \times d/4 \times e$  tiles (Figure 3b). For the tile- $ij$  scheme, tiles contain  $(d/2)(e)$  contiguous  $i$ -rows of only  $d/2$  elements each. For the tile- $j$  scheme, tiles contain  $e$  contiguous  $ij$ -planes of  $d^2/4$  elements each.

While the tile- $j$  scheme offers greater contiguity than the tile- $ij$  scheme in this example, even the  $j$ -tiles are not a single contiguous memory region with the  $ijk$ -layout. The only way to obtain completely contiguous tiles in the  $ijk$ -layout would be to tile the dimension with the greatest stride ( $k$ ), which is not an option as we never partition the small vertical dimension.

This limitation led us to the  $ikj$ -layout for the SSTA solver (see §V-A). With this layout, the direction of vectorization ( $i$ ) is still the unit stride dimension, avoiding strided loads and facilitating hardware prefetching. Additionally, the  $j$ -tiles are completely contiguous regions of memory, decreasing TLB pressure, increasing locality for caching and facilitating hardware prefetching.

Consider switching to the  $ikj$ -layout in the previous example. The  $ij$ -tiles would be the same as before:  $d/2 \times d/2 \times e$  tiles consisting of  $(d/2)(e)$  contiguous  $i$ -rows of only  $d/2$  elements each (Figure 3c). However, the  $j$ -tiles would be one contiguous region containing all  $(d^2/4)(e)$  elements (Figure 3d).

The only notable downside to the tile- $j$  scheme is the loss of flexibility in tile sizes. The smallest tile size for the tile- $j$  scheme is a  $d \times 1 \times e$  tile (an  $ik$  plane), while the smallest tile size for the tile- $ij$  scheme is a  $1 \times 1 \times e$  tile (a single column). We have not found this restriction to be problematic.

We present results from SSTA with the tile- $j$  scheme and both the  $ijk$ - and  $ikj$ -layout in this paper (see §V-A).

## IV. EXPERIMENTAL SETUP

We developed the Tridiagonal Solve Benchmarks (TSB) suite during the course of our research [22]. The TSB suite is freely available on Github under the Boost Software License, version 1.0. Git tag `ssta_paper_09_2016` contains the source code used for the experiments in this paper.

### A. Test Problem

The benchmarks in the TSB suite solve a vertical diffusion test problem on a 3D Cartesian grid with a time-stepping method. Each time-step, a matrix derived from the implicit Backward Time, Centered Space (BTCS) finite difference stencil with Dirichlet boundary conditions is solved in each vertical column. The diagonally-dominant tridiagonal matrix takes the following form, where  $D$  is a dimensionless diffusion coefficient ( $D > 0$ ),  $\Delta t$  is the time step size,  $\Delta k$  is the vertical grid spacing and  $r = D\Delta t/(\Delta k)^2$ :

$$A = \begin{bmatrix} 1 & 0 & & 0 \\ -r & 1+2r & -r & \\ & \dots & \dots & \dots \\ & & -r & 1+2r & -r \\ 0 & & & 0 & 1 \end{bmatrix}$$

An identical form of the problem is initialized in every vertical column of the grid and a matrix is constructed for each vertical solve.

### B. Hardware Platforms

The TSB suite currently targets x86-64 micro-architectures with SIMD vector units running POSIX-compliant operating systems. The results presented in this paper were collected from both Intel Xeon and Xeon Phi systems.

Our two Intel Xeon platforms, Edison and Cori Phase 1, are homogeneous Cray supercomputers, consisting of traditional dual-socket x86-64 nodes [23]. Edison features Intel Xeon E5-2695 v2 Ivy Bridge (IVB) processors [24]; Cori Phase 1 has Intel Xeon E5-2698 v3 Haswell (HSW) processors [25]. Both Xeon platforms have a very similar performance profile for our benchmark. In all experiments we restricted ourselves to a single socket.

Our Xeon Phi testbed, which features Intel Xeon Phi 7210 Knight’s Landing (KNL) processors [26], is notably different from the two Xeon systems. Knight’s Landing is a many-core design with a 2D mesh of **lightweight cores** optimized for throughput and parallelism at the expense of increased latency and reduced complexity in other areas (branch prediction, out-of-order execution facilities, pipeline depth, etc). The KNL micro-architecture has a number of novel features including on-package high-bandwidth MCDRAM, four hyper-threads per core and two AVX512 vector units per core. [27], [28]

Knight’s Landing processors can be configured for different Non-Uniform Memory Access (NUMA) topologies. Additionally, the MCDRAM can be configured as either programmable memory or a direct-mapped last-level cache [28]. For all experiments in this paper, we used a `quadcache` [27] configuration, where all cores are in a single NUMA domain and all 16GB of MCDRAM are used as a cache.

### C. Toolchain

TSB is written in ISO C++14 [29] and has no external software dependencies. The code contains no vector intrinsics or assembly. We rely entirely on the compiler vectorization engine for performant vector code generation, utilizing compiler directives and builtins to guide parallelization and vectorization, and indicate alignment, loop trip count and aliasing assumptions.

SSTA is task-parallelized using OpenMP `#pragmas` [30]. Since the problem is embarrassingly parallel in the horizontal dimensions, it is easy to statically load balance.

The Intel C++ Compiler [31] was used to compile the TSB suite for all of the results presented in this paper. We used the 2017 Beta Update 2 version (17.0.0 20160517). We also used the Intel VTune Amplifier XE profiler [19] during our research.

### D. Statistical Considerations

As described in §III-A, **effective bandwidth** is our primary performance metric. We define effective bandwidth as **effective data movement / solver execution time**.

We use our theoretical peak performance model to estimate effective data movement. To measure solver execution time, we record and average the wall-clock execution time of each time-step. We include OpenMP parallelization in our measurements, e.g. we time the `#pragma omp for` loop instead of measuring the duration of each tile-iteration individually. Thus, parallel overheads are included in our recorded execution times.

We performed each individual experiment a statistically significant number of times on different nodes of our test systems. Sample sizes varied between experiments and platforms, but were usually between 100 to 200 independent executions per data point. We estimated variance between different executions of the benchmark with identical parameters by computing sample standard deviation. Then we constructed **95% confidence intervals** (depicted visually with bars on all graphs) from the mean and sample standard deviation.

We used STREAM Triad [9] results as a reference for peak effective bandwidth. We measured a STREAM Triad bandwidth between 49.74 GB/s and 49.86 GB/s on our Ivy Bridge system, between 60.36 GB/s and 60.44 GB/s on our Haswell system and between 418.2 GB/s and 419.6 GB/s on our Knight's Landing system.

We believe there are two potential sources of non-trivial **systemic observational error** in our results.

First, mistakes in our analytic performance model for data movement could have introduced errors. We mitigated this by verifying the model with the Intel VTune Amplifier XE profiler [19], and we are confident in its validity.

Second, variance in the execution time of individual time-steps is not accounted for. We currently average the execution time of all time-steps within a single run of a benchmark, but do not compute and record sample standard deviation as a variance estimation within the solver. Removing this source of systemic error would be straightforward, but would require extending our post-processing framework to compute running sample standard deviations [32] which we have not yet implemented.

## V. RESULTS

We developed SSTA to replace the MKL-based vertical column solver in our production climate application because we believed better vectorization and data movement could be achieved by solving multiple vertical columns **simultaneously**. We also theorized that such a solver would be highly sensitive to **data layout changes** and **total tile size** (§III-D).

Parallel application performance is often driven by parameters such as tile size, which control the amount of work in each parallel task. In memory-bandwidth bound applications, data layout and tiling can be especially important as they not only influence the amount of task- and vector-parallelism exposed but also the working set size and degree of cached data reuse in each individual task. We anticipated that we would need to study the effect of different data layouts and tile sizes in order to understand the performance of our new solver. The first step was to determine the **optimal total tile size** for the different solver variants in the TSB suite.

We conducted a parameter sweep of total tile size on our Xeon and Xeon Phi platforms. We predicted that we would see the following:

- The MKL baseline solver would be insensitive to total tile size, excluding extremely small (high overhead) and extremely large (insufficient parallelism) tile sizes, since it solves each column independently and thus cannot exploit vector instructions and data locality like the SSTA solver does.
- Total tile sizes small enough to fit into the L1D cache would not be feasible because the overheads of loops and parallelization would be too great relative to the execution time of useful work per inner-loop iteration. These tile sizes would either require vertical extents below the sizes we are interested in ( $nk < 16$ ) or horizontal extents too small to vectorize efficiently ( $ni < 16$ ).
- The optimal total tile size would fit into the L2 cache, but not the L1D, since the L2 is the fastest cache that has the capacity to contain a feasible tile size.
- Excluding the L1D, as we move from a tile size that fits into the capacity of a particular cache to a tile size that does not, we should see a drop in effective bandwidth. On the Xeon platforms, the boundaries are  $L2 \rightarrow L3$  and  $L3 \rightarrow \text{DRAM}$  (main memory). On Knight's Landing, the boundaries are  $L2 \rightarrow \text{MCDRAM}$  cache and  $\text{MCDRAM cache} \rightarrow \text{DRAM}$  (main memory).

Note that when a total tile size is exactly equal to a particular cache capacity, we claim that it will not fit into that cache.

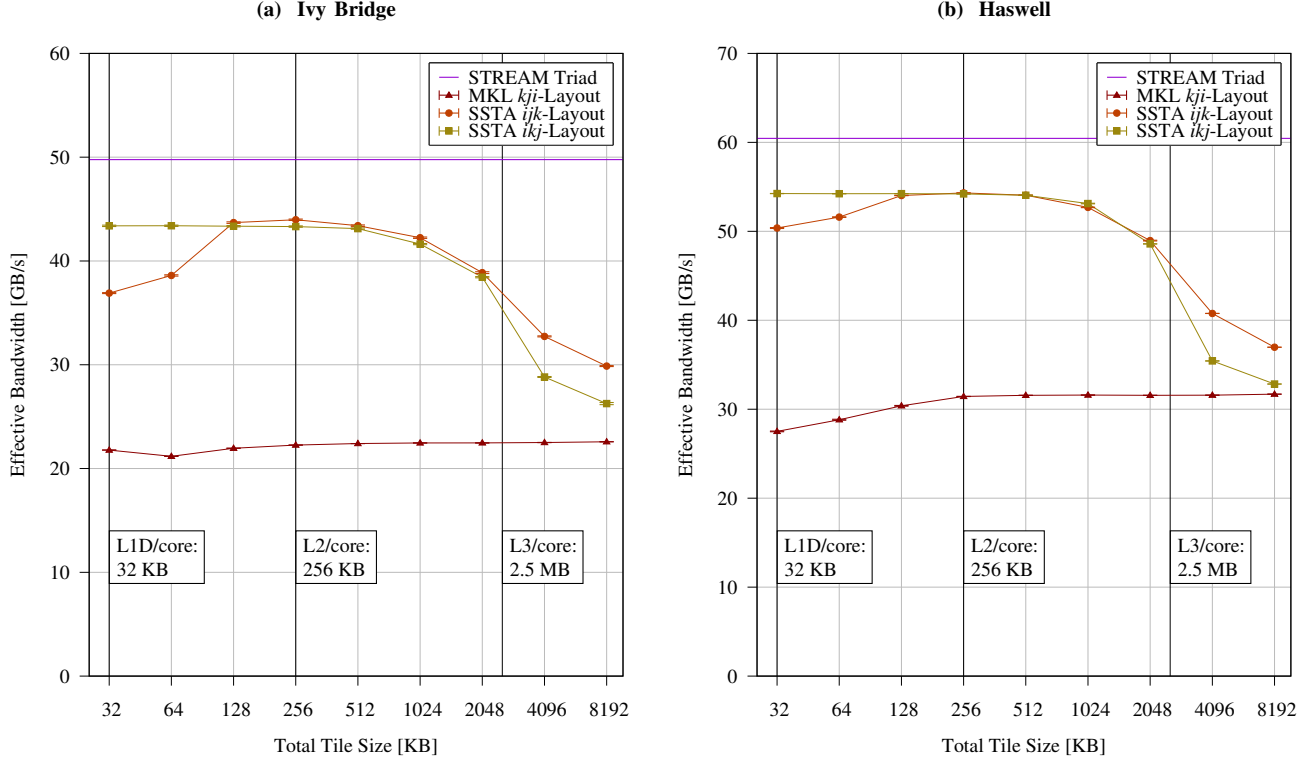
The results of this parameter sweep for both the  $ijk$ - and  $ikj$ -layout are shown in Figure 4a (Ivy Bridge), Figure 4b (Haswell) and Figure 5 (Knight's Landing). Results from the TSB suite's MKL baseline solver are shown as a lower bound, and STREAM Triad results are shown as an upper bound. A  $32 \times 147456 \times 32$  grid of double precision floating point values was used on all platforms (4.5GB in total for  $a$ ,  $b$ ,  $c$  and  $u$ ). All results were run on a full socket, with one application-thread bound to each core.

### A. Analysis

We found that the MKL baseline solver was largely insensitive to tile size, as predicted. Across the range of total tile



**Figure 4: SSTA Effective Bandwidth vs. Total Tile Size:** The results of a parameter sweep on our two Intel Xeon platforms demonstrating the effect of total tile size on the performance of the SSTA solver is shown below (MKL baseline and STREAM Triad results shown as lower- and upper-bounds). The *ikj*-layout, which exhibits better contiguity and memory access patterns, performs better at smaller tile sizes, although the best *ikj*-layout result does not outperform the best *ijk*-layout result on these platforms. Performance degrades for tile sizes that exceed L3 capacity per core. Both SSTA variants substantially outperform the MKL baseline results and reach ~90% of STREAM Triad effective bandwidth with optimal tile sizes. Results are shown with 95% confidence (see §IV-D).



sizes we tested, we did not observe performance variation that was statistically significant enough to distinguish it from random observational error, which is what we anticipated.

As we predicted, total tile sizes small enough to fit into the L1D cache were impractical on all platforms. We would have to either reduce the vertical extent or the horizontal extent  $ni$  to generate a tile size small enough to fit into the 32KB L1D with the tile- $j$  scheme. We ran preliminary experiments with  $ni = 16$  (not shown) to observe the effect of 16KB tile sizes. The results indicated that tile sizes smaller than 32KB performed worse for both the *ijk*- and *ikj*-layouts on all platforms. At  $ni = 16$ , the trip count on some of the loops in SSTA is so small that the compiler cannot perform as much unrolling post-vectorization as it would for larger  $i$  extents.

On Knight’s Landing, the optimal total tile size for the SSTA *ijk*-layout variant is 128KB, which is small enough to fit within the L2 but too large for the L1D. On Ivy Bridge and Haswell, the optimal total tile size for the *ijk*-layout is 256KB, which is too large for the L2. While it is difficult to distinguish between the 128KB, 256KB and 512KB results in Figures 4a and 4b because the magnitude of the difference is relatively small, the confidence intervals do not overlap and the trend of the dataset supports our conclusion.

We were intrigued to find that, contrary to our predictions,

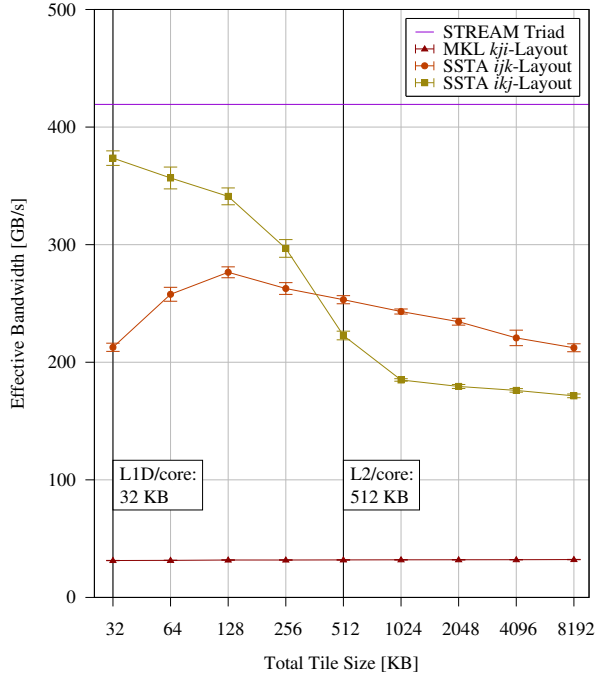
the optimal total tile size for the *ijk*-layout on the Xeon platforms was too large to fit within the L2. Additionally, while the optimal total tile size for the *ijk*-layout on Knight’s Landing would fit within the L2 cache, performance was not as close to peak as it was on the Xeon platforms (see Table II).

Profiling indicated that the SSTA *ijk*-layout variant experienced a high number of L1 DTLB store misses. As we decreased total tile size, we observed progressively worse TLB performance in our profiling traces. We determined this was due to the lack of fully contiguous tiles in the *ijk*-layout (see §III-D). As the tile size is decreased, the size of each contiguous plane decreases and the frequency of non-contiguous jumps through memory increases, negatively impacting TLB, cache and hardware prefetching performance, especially on Knight’s Landing (See Figure 5).

We conducted a parameter sweep with the SSTA *ijk*-variant and a smaller vertical extent ( $nk = 16$ , not shown) to further verify the cause of this issue. With fewer vertical levels, the number of contiguous regions for each tile size would be decreased and the size of each contiguous region would be increased, improving contiguity. We observed performance improvements with  $nk = 16$ ; on Knight’s Landing the impact was significant.

The poor performance of the *ijk*-layout on Knight’s

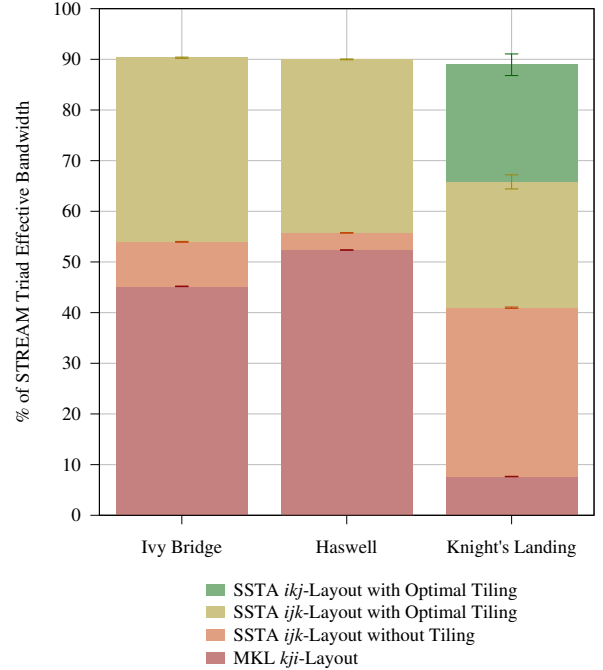
**Figure 5: SSTA Effective Bandwidth vs. Total Tile Size (Knight’s Landing):** Shown below are the results of a parameter sweep on our Intel Xeon Phi Knight’s Landing platform showing the effect of data layout and total tile size on the performance of the SSTA solver. MKL baseline (lower-bound) and STREAM Triad (upper-bound) results are shown for reference. *ijk*-layout performance is hampered by poor data contiguity that incurs expensive TLB and hardware prefetching penalties on Knight’s Landing. This effect is amplified at smaller tile sizes. The best *ikj*-layout result has between 91 GB/s and 109 GB/s higher effective bandwidth than the best *ijk*-layout result, and reaches between 88% and 92% of STREAM Triad performance. Results are shown with 95% confidence (see §IV-D).



Landing led us to develop the *ikj*-layout variant of SSTA described in §III-C and §III-D. The optimal total tile size for the *ikj*-layout was 32KB on all three platforms. On the Xeon platforms, the best *ikj*-layout result does not outperform the best *ijk*-layout result, although the *ikj*-layout variant does perform better than the *ijk*-layout variant at smaller tile sizes. However, on Knight’s Landing the best *ikj*-layout result achieves between 91 GB/s and 109 GB/s higher effective bandwidth than the best *ijk*-layout result (see Table II), a significant improvement.

Our prediction that the optimal total tile size would be larger than L1D capacity but smaller than L2 capacity held for the *ikj*-layout on all platforms and also for the *ijk*-layout on Knight’s Landing. For the *ijk*-layout on the Xeon platforms, the optimal total tile size was too large to fit into the L2. We believe the difference between optimal total tile sizes on the Xeon platforms and Knight’s Landing is due to the lack of a traditional L3 cache on the latter, making the performance penalty greater for L2 misses. We can draw the conclusion that, for the platforms surveyed, the optimal total tile size for the *ijk*-layout is large enough to reside in the last-level associative on-die cache (the L3 on the Xeon

**Figure 6: Percentage of STREAM Triad Effective Bandwidth Attained by SSTA:** Across all three micro-architectures, the SSTA solver with an optimal total tile size improves performance substantially over the MKL baseline, and achieves ~90% of STREAM Triad effective bandwidth. Although untiled SSTA results beat the MKL solver, tiling contributes significantly to overall performance: between 35.9% and 36.1% on Ivy Bridge, between 34.22% and 35.38% on Haswell and between 24% and 26% on Knight’s Landing. Between 21% and 25% of STREAM performance attained is attributed to the switch to the *ikj*-layout on Knight’s Landing. Results are shown with 95% confidence (see §IV-D).



platforms and the L2 on Knight’s Landing).

The total tile size parameter sweep mostly supports our prediction that performance drops when going from tile sizes that fit into a particular cache to tile sizes that do not. We see no such decrease at the L2 capacity boundary on the Xeon platforms, but we do see a drop when the tile size exceeds L3 capacity per core. On Knight’s Landing, we see a drop as we cross the L2 capacity boundary. We posit that a modified version of our prediction is more accurate; as we move from a tile size that will fit into the last-level associative on-die cache to a tile size that will not, there is a drop in SSTA’s effective bandwidth.

## VI. CONCLUSION

We introduced the Simultaneous Streaming Thomas Algorithm (SSTA) solver, which can efficiently solve many small tridiagonal matrix systems simultaneously, and addresses a performance bottleneck that arises in a number of scientific application domains. We have demonstrated the impact of different tiling schemes, tile sizes and data layouts, and how they interact with the memory sub-system.

We found that the *ijk*-layout version of SSTA provides the best performance on Xeon platforms with a total tile size that is small enough to fit into the L3 cache but is too



Table II: **Summary of SSTA Performance Results:** SSTA outperforms the MKL baseline solver on all of our test platforms. SSTA achieves a  $\sim 2x$  speedup over the MKL solver on our Xeon platforms, a  $\sim 12x$  speedup on Knight’s Landing, and attains  $\sim 90\%$  of STREAM Triad effective bandwidth on all three platforms. All measurements are reported with 95% confidence (see §IV-D).

Solver	Optimal Total Tile Size	Effective Bandwidth Bandwidth	Percentage of STREAM TRIAD Bandwidth	Speedup vs. MKL
<b>Ivy Bridge</b>				
MKL <i>kji</i> -layout	Any	$22.49 \pm 0.003$ GB/s	$45.2 \pm 0.05$ %	1 <i>x</i>
SSTA <i>ijk</i> -layout	256 KB	$44.0 \pm 0.07$ GB/s	$90 \pm 0.1$ %	$\sim 2$ <i>x</i>
SSTA <i>ikj</i> -layout	32 KB	$43.0 \pm 0.07$ GB/s	$87 \pm 0.2$ %	$\sim 1.9$ <i>x</i>
<b>Haswell</b>				
MKL <i>kji</i> -layout	Any	$31.65 \pm 0.006$ GB/s	$52.4 \pm 0.04$ %	1 <i>x</i>
SSTA <i>ijk</i> -layout	256 KB	$54.3 \pm 0.01$ GB/s	$90.0 \pm 0.07$ %	$\sim 1.7$ <i>x</i>
SSTA <i>ikj</i> -layout	32 KB	$54.2 \pm 0.01$ GB/s	$89.7 \pm 0.06$ %	$\sim 1.7$ <i>x</i>
<b>Knight’s Landing</b>				
MKL <i>kji</i> -layout	Any	$32 \pm 0.2$ GB/s	$7.6 \pm 0.04$ %	1 <i>x</i>
SSTA <i>ijk</i> -layout	128 KB	$280 \pm 5$ GB/s	$66 \pm 1$ %	$\sim 9$ <i>x</i>
SSTA <i>ikj</i> -layout	32 KB	$370 \pm 6$ GB/s	$90 \pm 2$ %	$\sim 12$ <i>x</i>

large to fit in the L2. On Knight’s Landing, the *ikj*-layout yields the best performance with a tile size that is small enough to fit in the L2.

Our results are summarized in Table II. They show that SSTA is a highly efficient solver capable of achieving 90% of STREAM Triad bandwidth on Intel Xeon and Xeon Phi systems, including the new Knight’s Landing micro-architecture. Our algorithm is a substantial improvement over the MKL-based *kji*-layout baseline solver; it is  $\sim 2x$  faster on Xeon platforms and  $\sim 12x$  faster on Knight’s Landing.

## VII. FUTURE WORK

There are also a number of optimizations that we developed for the SSTA solver but have not presented here. The version of the TSB suite described in this paper uses what we refer to as the **full-grid scheme**, where the tridiagonal matrix is built and stored for all vertical columns. The alternative **rolling-grid scheme** builds the matrix on the fly in a tile-sized  $a$ ,  $b$  and  $c$ . In addition to offering storage savings, we believe the rolling-grid scheme will further improve data locality and hardware prefetching performance as the storage for the matrix will be reused for all tiles that a core executes (each column’s matrix may still be different). Further research is also needed to explore smaller total tile sizes, as well as the tile-*ij* scheme, as it may be beneficial to production applications that are willing to accept some performance trade-off for increased flexibility in the extent of the horizontal dimension  $i$ .

We would like to extend the range of hardware platforms and configurations in future experiments. On Knight’s Landing, further effort is needed to study the trade-off between utilizing MCDRAM as a cache versus programmable memory. We are also interested in testing SSTA on SIMT GPGPU architectures.

There are also a number of related numerical problems that we believe could be addressed by some of the techniques we describe in this paper. The algorithm could be extended to include matrix assembly based on solution values and put

inside a fully non-linear iteration with a Jacobian calculation, such as those used in Newton iterations. The challenge here is that some vertical columns may converge faster than others, which may require vector masking or scalar iterative refinement. Opportunities to extend the algorithm to banded or other sparse matrices and incomplete LU-type algorithms are straight-forward for diagonally-dominant cases, but pivoting has the potential to hinder vectorization and memory access patterns.

Finally, more complex multi-kernel applications integrate multiple solvers and computational phases, such as traditional finite difference stencil operations and time integration algorithms. We will have to explore the performance trade-offs between the *ijk*-, *kji*- and *ikj*-layouts in these applications.

Our efforts in the immediate future will revolve around research into those trade-offs and the integration of SSTA into our production software.

## ACKNOWLEDGMENTS

This material is based upon work supported by the U.S. Department of Energy Office of Science’s Scientific Discovery through Advanced Computing (SciDAC) program and the Intel Parallel Computing Center (IPCC) at Lawrence Berkeley National Laboratory (LBNL). Resources at the National Energy Research Scientific Computing Center (NERSC), which is supported by the U.S. Department of Energy Office of Science’s Advanced Scientific Computing Research (ASCR) program (contract DE-AC02-05CH11231), were used to produce this work.

Our thanks to Cy Chan for providing early feedback and identifying a serious error in Figure 3c.

## REFERENCES

- [1] A. Gettelman and H. Morrison, “Advanced Two-Moment Bulk Microphysics for Global Models Part I: Off-Line Tests and Comparison with Other Schemes,” *Journal of Climate*, vol. 28, no. 3, pp. 1268–1287, 2015, <https://goo.gl/ZRgxbk>.
- [2] W. E. Pazner, A. Nonaka *et al.*, “A High-Order Spectral Deferred Correction Strategy for Low Mach Number Flow with Complex Chemistry,” *Combustion Theory and Modelling*, vol. 20, no. 3, pp. 521–547, 2016, <https://goo.gl/JWCdFf>.
- [3] M. J. Iacono, J. S. Delamere *et al.*, “Radiative Forcing by Long-Lived Greenhouse Gases: Calculations with the AER Radiative Transfer Models,” *Journal of Geophysical Research: Atmospheres*, vol. 113, no. D13, 2008, <https://goo.gl/pgghJC>.
- [4] G. Tang, F. Yuan *et al.*, “Addressing Numerical Challenges in Introducing a Reactive Transport Code into a Land Surface Model: a Biogeochemical Modeling Proof-of-Concept with CLM-PFLOTRAN 1.0,” *Geoscientific Model Development*, vol. 9, no. 3, pp. 927–946, 2016, <https://goo.gl/NzayJx>.
- [5] M. Khairoutdinov, D. Randall, and C. DeMott, “Simulations of the Atmospheric General Circulation using a Cloud-Resolving Model as a Superparameterization of Physical Processes,” *Journal of the Atmospheric Sciences*, vol. 62, no. 7, pp. 2136–2154, 2005, <https://goo.gl/h3zMzR>.
- [6] H. Weller, S.-J. Lock, and N. Wood, “Runge-Kutta IMEX Schemes for the Horizontally Explicit/Vertically Implicit (HEVI) Solution of Wave Equations,” *Journal of Computational Physics*, vol. 252, pp. 365–381, 2013, <https://goo.gl/RJRSU1>.
- [7] Intel Math Kernel Library (MKL). <https://goo.gl/ZzbZ5B>.
- [8] NVIDIA CUDA BLAS Library (cuBLAS). <https://goo.gl/nB4IO5>.
- [9] J. D. McCalpin, “Memory Bandwidth and Machine Balance in Current High Performance Computers,” *IEEE Computer Society Technical Committee on Computer Architecture (TCCA) Newsletter*, pp. 19–25, dec 1995, <https://goo.gl/2hLwKz>.
- [10] K. Iglberger, G. Hager *et al.*, “High Performance Smart Expression Template Math Libraries,” in *Proceedings of the International Conference on High Performance Computing Simulation*, 2012, pp. 367–373, <https://goo.gl/WtLiSW>.
- [11] Blaze source code repository. <https://goo.gl/3l0D3t>.
- [12] A. Heinecke, G. Henry *et al.*, “LIBXSMM: Accelerating Small Matrix Multiplications by Runtime Code Generation,” in *Proceedings of the International Conference for High Performance Computing, Networking, Storage and Analysis*, 2016, pp. 84:1–84:11, <https://goo.gl/AqtHvm>.
- [13] LIBXSMM source code repository. <https://goo.gl/CDTP9K>.
- [14] A. Povitsky, *Parallelization of the Pipelined Thomas Algorithm*. Institute for Computer Applications in Science and Engineering (ICASE), 1998, <https://goo.gl/tO0Z23>.
- [15] A. Haidar, T. Dong *et al.*, “Optimization for Performance and Energy for Batched Matrix Computations on GPUs,” in *Proceedings of the 8th Workshop on General Purpose Processing Using GPUs*, 2015, pp. 59–69, <https://goo.gl/QecWej>.
- [16] S. D. Conte and C. W. D. Boor, *Elementary Numerical Analysis: An Algorithmic Approach*, 3rd ed. McGraw-Hill Higher Education, 1980, <https://goo.gl/E5qKGA>.
- [17] S. Williams, A. Waterman, and D. Patterson, “Roofline: An Insightful Visual Performance Model for Multicore Architectures,” *Communications of the ACM*, vol. 52, no. 4, pp. 65–76, 2009, <https://goo.gl/AtCEcG>.
- [18] *Intel 64 and IA-32 Architectures Software Developers’ Manual*, 325383-059US ed., 2016, <https://goo.gl/OzZKIA>.
- [19] Intel VTune Amplifier XE. <https://goo.gl/F218Pw>.
- [20] M. D. Lam, E. E. Rothberg, and M. E. Wolf, “The Cache Performance and Optimizations of Blocked Algorithms,” *ACM SIGPLAN Notices*, vol. 26, no. 4, pp. 63–74, 1991, <https://goo.gl/6HGE4Y>.
- [21] H. C. Edwards, C. R. Trott, and D. Sunderland, “Kokkos: Enabling Manycore Performance Portability through Polymorphic Memory Access Patterns,” *Journal of Parallel and Distributed Computing*, vol. 74, no. 12, pp. 3202–3216, 2014, <https://goo.gl/3heOLi>.
- [22] Tridiagonal Solve Benchmarks (TSB) suite source code repository. <https://goo.gl/iuhHst>. Available under the Boost Software License 1.0 (a BSD-style open source license).
- [23] National Energy Research Scientific Computing Center (NERSC) Systems. <https://goo.gl/0OgfcP>.
- [24] Intel Xeon Processor E5-2695 v2 (30M Cache, 2.40 GHz) Specifications. <https://goo.gl/84vkJd>.
- [25] Intel Xeon Processor E5-2698 v3 (40M Cache, 2.30 GHz) Specifications. <https://goo.gl/t0GdZr>.
- [26] Intel Xeon Phi Processor 7210 (16GB, 1.30 GHz, 64 core) Specifications. <https://goo.gl/xLtmjm>.
- [27] D. Doerfer, J. Deslippe *et al.*, “Applying the Roofline Performance Model to the Intel Xeon Phi Knights Landing Processor,” in *Intel Xeon Phi User Group Workshop Annual US Meeting*, 2016, <https://goo.gl/UW11Ks>.
- [28] A. Sodani, “Knights Landing (KNL): 2nd Generation Intel Xeon Phi Processor,” in *27nd Hot Chips Symposium*, 2015, <https://goo.gl/AkIzBk>.
- [29] *ISO/IEC 14882:2014, Standard for Programming Language C++*, 2014, <https://goo.gl/bCZsW>.
- [30] *OpenMP Specification Version 4.5*, 2015, <https://goo.gl/QaZ1FD>.
- [31] Intel C++ Compiler. <https://goo.gl/Vf7VII>.
- [32] B. Adelstein Lelbach, “Benchmarking C++ Code,” in *C++Con 2015*, 2015, <https://goo.gl/S83V34>.